Chemical Science

EDGE ARTICLE

View Article Online
View Journal | View Issue

Cite this: *Chem. Sci.*, 2019, **10**, 4163

All publication charges for this article have been paid for by the Royal Society of Chemistry

Water-soluble chiral tetrazine derivatives: towards the application of circularly polarized luminescence from upper-excited states to photodynamic therapy†

Tingchao He,[a] Can Ren,[a] Yu Luo,[b] Qi Wang,[c] Junzi Li,[a] Xiaodong Lin,[a] Chuanxiang Ye,[a] Wenbo Hu*[c] and Junmin Zhang*[b]

Received 17th January 2019
Accepted 7th March 2019

DOI: 10.1039/c9sc00264b

rsc.li/chemical-science

A new family of water-soluble chiral tetrazine derivatives **1** and **2** is reported. Spectroscopic studies reveal that the derivatives violate Kasha's rule and emit from their upper-excited states (S_n, $n > 1$). The transition assignments are supported by time-dependent density functional theory calculations. More importantly, both chromophores exhibit anisotropy factors on the order of $\sim 10^{-3}$ to 10^{-4} for circular dichroism and circularly polarized luminescence (CPL) from upper-excited states. Additionally, the nonplanar geometry of the derivatives induces a significant yield of triplet excited states. Transient absorption spectroscopic measurements reveal high triplet quantum yields of ~86% for **1** and ~81% for **2**. Through *in vitro* studies, we demonstrate that the derivatives can be used as photodynamic therapy (PDT) agents, providing a highly efficient form of cancer therapy. This study is the first demonstration of simple organic molecules with CPL from upper-excited states and efficient PDT.

Introduction

When the energy gap between short- and long-wavelength bands becomes sufficiently large, a slow internal conversion process between upper-excited states (S_n, $n > 1$) and S_1 excited states is expected.[1–6] In this case, some molecules display weak emission from the S_n state to the S_0 state. Contrary to Kasha's rule, molecules that emit S_n fluorescence are rare but are particularly promising in photovoltaic cells and optically operated logic gates.[7] Furthermore, investigating the photophysical properties in the S_n states is very important and challenging because many energy and electron transfer processes occur in the initial S_n states, and the deactivation process from the S_n states is relatively rapid. Several types of organic molecules including porphyrin-based systems,[1–5] boron dipyrromethene derivatives,[6] azulene,[8] and thiones[9] have received much attention because of their peculiar S_2 emission properties. Although some papers report general fluorescence emission from S_n states,[1–6] circularly polarized luminescence (CPL) from S_n states has not yet been developed. Interest in CPL has grown in recent years, especially because of its utilization as a source of information about the chiral structures of emitting excited states, as well as its potential for smart photonic applications such as 3D displays and information storage.[10–15] In particular, the development of CPL from S_n states may increase the number of potential applications of chiral materials. Despite their promising application background, such organic molecules are still scarce and are practically unknown. There are two effective ways to achieve molecular chirality. One way is to tether a perturbing chiral moiety to an inherently achiral organic chromophore.[14] The other way is to fabricate achiral organic molecules into chiral building blocks, such as double helices, twists, and rolled-up nanotubes.[16] Although the first way is less efficient relative to the second, it is more useful for some special CPL-related applications, *e.g.*, biomolecular CPL sensing in cells and smart photonic devices. If the achiral molecules with emission from upper-excited states are perturbed with chiral moieties, CPL from the upper-excited states should be achieved.

It should be noted that the dynamic processes of these organic molecules are affected by not only the energy gap but also intersystem crossing (ISC), which is a key factor for the application of photodynamic therapy (PDT).[17–19] Although the fluorescence emission from S_n states and the ISC properties of simple molecules have been studied separately, the combination of CPL from S_n states and efficient ISC into these states remains absent in the literature. Therefore, the design and

[a]College of Physics and Energy, Shenzhen University, Shenzhen 518060, China
[b]College of Chemistry and Environmental Engineering, Shenzhen University, Shenzhen 518060, China. E-mail: zhangjm@szu.edu.cn
[c]Key Laboratory of Flexible Electronics (KLOFE), Institute of Advanced Materials (IAM), Jiangsu National Synergetic Innovation Center for Advanced Materials (SICAM), Nanjing Tech University (NanjingTech), Nanjing 211816, China. E-mail: iamwbhu@njtech.edu.cn

† Electronic supplementary information (ESI) available: Experimental details of synthesis, characterization and supplementary figures. See DOI: 10.1039/c9sc00264b

synthesis of such special, simple molecules may open up new avenues for their use in various applications, such as in photovoltaics and biological science, as well as in new fields that are currently under exploration. There are also two ways to achieve efficient ISC in organic molecules. One way is to introduce heavy metals to enhance molecular spin–orbit coupling; the other way is to reduce the energy gap between the singlet and triplet states.[20] The latter can be realized through the incorporation of curved (nonplanar) π-electron systems into the organic molecules.[21–24] Hence, the combination of CPL from S_n states and efficient ISC from the singlet to the triplet states may be achieved in twisted molecular architectures that are perturbed with chiral moieties and have a sufficiently large energy gap between the S_n and S_1 states.

In this work, we have designed and synthesized the enantiomeric twisted tetrazine derivatives 1-*R*, 1-*S*, 2-*R* and 2-*S* as evidence of the workability of a new simple structural design. (*R* or *S*)-1-Phenylethyl-amine and (*R* or *S*)-2-aminohexane were tethered to the achiral tetrazine core to form new chiral tetrazine derivatives 1-*R*, 1-*S*, 2-*R* and 2-*S*, respectively. Additionally, the derivatives exhibit a large energy gap between the S_n and S_1 states. More interestingly, the water-soluble, simple organic molecules represent the first example of chiral molecules enabling CPL from S_n states, which can be exploited to generate exceptional ISC in PDT.

Results and discussion

Tetrazine derivatives 1-*R*, 1-*S*, 2-*R* and 2-*S* were straightforwardly obtained from a commercially available 3,6-dichlorotetrazine core, by substitution with commercial (*R* or *S*)-1-phenylethylamine and (*R* or *S*)-2-aminohexane, respectively, according to a previously described method (Scheme 1).[25,26] Compounds **1** and **2** were characterized by ^{1}H NMR and ^{13}C NMR spectroscopy, and elemental analysis (Fig. S1–S4 in the ESI†). The obtained samples of **1** and **2** were not solid powders but liquids with high viscosity, so a single crystal of the derivatives cannot be easily obtained to confirm their absolute configurations. Previous literature reports have proven that the use of (*R* or *S*)-1-phenylethylamine and (*R* or *S*)-2-aminohexane as starting materials for similar transformations will not alter the absolute configuration of the resultant derivatives.[27–30] Therefore, the absolute configuration of chiral centres of the derivatives should be consistent with (*R* or *S*)-1-phenylethylamine and (*R* or *S*)-2-aminohexane, even though no single crystal X-ray analysis is provided. Compounds **1** and **2** can be dissolved easily in chloroform ($CHCl_3$) and water.

To investigate the electronic structures of the tetrazine derivatives **1** and **2**, their photophysical properties were investigated. As shown in Fig. 1a and b, both **1** and **2** display sharp absorption bands that correspond to S_0–S_n centred at 250 and 252 nm. The second broad bands (S_0–S_2) show vibronic features with maxima at 391 and 413 nm for **1**, and 397 and 417 nm for **2**. Additionally, the third broad absorption band (S_0–S_1) was observed for **1** and **2** peaking at 520 and 521 nm, respectively. The experimental absorption spectra can be reproduced well using time-dependent density functional theory (TDDFT B3LYP 631G**, Fig. S5†), and the relevant transitions can be further confirmed by the calculation of their oscillation strengths (Table S1†). The lowest energy singlet excited states were calculated to elucidate the nature of the electronic transitions that give rise to the absorption bands in the electronic spectra (Fig. 1). For chromophores **1** and **2**, TD-DFT predicts that the $S_0 \rightarrow S_1$ and $S_0 \rightarrow S_2$ bands are a HOMO → LUMO and a HOMO−1 → LUMO transition, respectively, whereas the $S_0 \rightarrow S_n$ band corresponds to a HOMO−1 → LUMO+1 transition (Fig. S6†).

Fluorescence studies performed on **1** and **2** revealed that the $S_1 \rightarrow S_0$ emission peaks were located at 565 and 564 nm, respectively, starting with a 521 nm excitation from the lowest energy $S_0 \rightarrow S_1$ band (Fig. 1). Importantly, for chromophore **1**, one dominant emission band other than the broad $S_1 \rightarrow S_0$ emission appeared, with three maxima at 433, 469 and 495 nm, starting with a 395 nm excitation that corresponds to the $S_0 \rightarrow S_2$ transition. This broad emission band for **1** was consistent in energy with an $S_2 \rightarrow S_0$ emission. Chromophore **2** displays the $S_2 \rightarrow S_0$ broad emission band with three maxima at 434, 468 and 496 nm. More interestingly, after a 250 nm excitation corresponding to the $S_0 \rightarrow S_n$ transition, another broad emission band was observed for both **1** and **2**. The broad emission band for **1** with a maximum at 345 nm correlates in energy with a radiative $S_n \rightarrow S_0$ deactivation, whereas the $S_n \rightarrow S_0$ broad emission band with a maximum at 311 nm was observed for chromophore **2**. To the best of our knowledge, this is the first observed $S_n \rightarrow S_0$ ($n > 2$) emission. According to Kasha's rule,

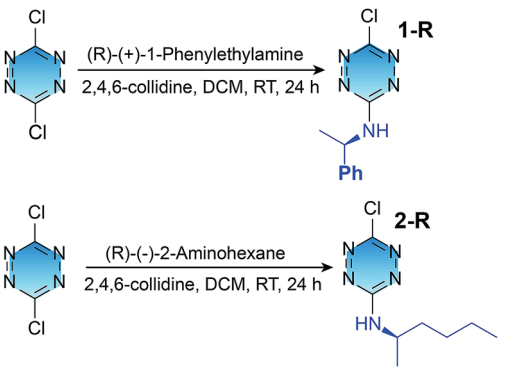

Scheme 1 Synthesis routine of water-soluble chiral tetrazine derivatives.

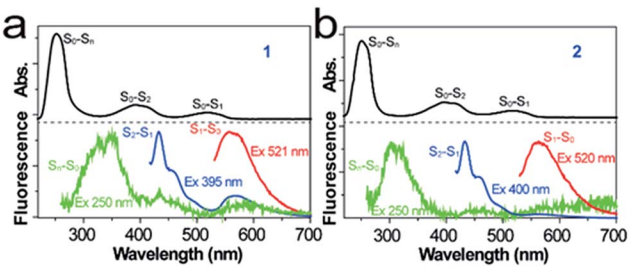

Fig. 1 Comparison of absorption and fluorescence spectra of (a) **1** and (b) **2** in $CHCl_3$ under excitation by different wavelengths.

the emitting electronic level of a molecule is usually its lowest excited level. However, in the case of a large energy gap between the S_n ($n > 1$) and S_1 states, which corresponds to their small S_n–S_1 vibrational overlap (Franck–Condon) factor, the nonradiative decay from the S_n state will be much slower. The fact that compounds **1** and **2** violate Kasha's rule can be attributed to the large S_2–S_1 and S_n–S_1 energy gaps. The energy gap values for S_2–S_1 (1.84 eV) and S_n–S_1 (2.58 eV) were estimated for **1**, which are comparable to the corresponding values of **2**, *i.e.*, S_2–S_1 (1.91 eV) and S_n–S_1 (2.57 eV). These values are among the largest for molecules that emit from the S_n ($n > 1$) level.[1–6] It is reasonable that the large S_2–S_1 and S_n–S_1 energy gaps of **1** and **2** lead to the violation of Kasha's rule, and thus to the emission from the S_2 and S_n levels. The fluorescence quantum yields of the S_1, S_2 and S_n emissions were determined to be 0.013%, 0.04% and 4.5×10^{-5}% for **1**, while the respective values were 0.025%, 0.08% and 6.4×10^{-5}% for **2**. The low fluorescence quantum yields of **1** and **2** should be mainly caused by the rapid deactivation process from the S_n states and high efficiency ISC from the singlet state to the triplet state, which will be discussed later.

To evaluate the chiroptical properties of the tetrazine derivatives, we measured their CD spectra. The entire CD spectra of 1-*R*, 1-*S*, 2-*R* and 2-*S* give clear mirror images, which extend from the extreme ultraviolet to visible bands (Fig. 2). The enantiopure 1-*R* and 1-*S* show opposite Cotton effects at 250 and 400 nm. Moreover, the maximum dichroic signals of the CD spectra match the maximum absorption of the chromophores. The maximum level of CD measured in terms of $|g_{abs}|$ was 3.2×10^{-3} at 290 nm, 4.1×10^{-4} at 400 nm and 4.8×10^{-5} at 520 nm for **1**, whereas the relevant values for **2** were 1.6×10^{-3} at 290 nm, 2.5×10^{-4} at 400 nm and 2.8×10^{-5} at 520 nm. These values were determined by the equation $g_{abs} = \Delta\varepsilon/\varepsilon = (A_L - A_R)/A$, where A represents the conventional absorption of non-polarized light and A_L and A_R are the absorption of left and right circularly polarized light, respectively.[31,32] Moreover, the simulated CD spectra of compounds **1** and **2** were compared with their experimental spectra and they basically reproduced the experimental features, especially in the high-energy part.

The strong CD response of **1** and **2** in their ground states makes their CPL possible. Considering the limit of the excitation wavelength of our CPL instrument (350–800 nm), we only measured the CPL properties of enantiopure **1** and **2** in $CHCl_3$ excited at 395 and 520 nm (Fig. 3). As expected, upon excitation at 520 nm, **1** and **2** indeed exhibited CPL activities from the S_1 state, whereas CPL from the S_2 state was observed after excitation at 395 nm. The recorded CPL spectra are virtually mirror images, whose maxima match the maximum emissions of **1** and **2**. The dissymmetric factor for luminescence, $|g_{lum}|$, which is defined as $g_{lum} = 2(I_L - I_R)/(I_L + I_R)$, where I_L and I_R are the intensities of left and right fluorescence emission,[31,32] was estimated to be 7.9×10^{-4} for **1** and 4.5×10^{-4} for **2** when excited at 395 nm. When excited at 520 nm, the values of $|g_{lum}|$ were determined to be 7.2×10^{-5} for **1** and 4.9×10^{-5} for **2**. Although the values of $|g_{lum}|$ are relatively small, they prove, for the first time, the feasibility of achieving CPL with simple molecules, especially from the S_n state. Although we have not measured the CPL spectra of **1** and **2** upon excitation at 250 nm, it is highly expected that CPL activities from S_n can be achieved, considering their strong CD signals that correspond to the S_0–S_n transition.

To unravel the kinetics of the ISC, the chromophores 1-*R* and 2-*R* in $CHCl_3$ were excited at 400 nm with a 100 fs laser pulse. Full contour plots of fs-TA spectra of 1-*R* and 2-*R* are shown in Fig. 4a and b, respectively. Fs-TA spectra of 1-*R* and 2-*R* at various pump–probe delay times are plotted in Fig. 4c and d. Chromophore 1-*R* exhibits positive absorption peaks centred at 381, 447, 490, 546 and 607 nm, whereas positive absorption peaks centred at 385, 457, 488, 546 and 610 nm are observed for 2-*R*. Remarkably, for 1-*R* (2-*R*), accompanied by the decay of the band at 607 nm (610 nm), another positive band peak at 490 nm (488 nm) gradually appears. Positive absorption centred at 607 nm (610 nm) corresponds to singlet–singlet transitions, whereas the positive absorption band at 490 nm (488 nm) is ascribed to the triplet–triplet transition. For more underlying information, the fs-TA profiles and kinetic traces at the wavelengths of the singlet and triplet states were extracted and are presented in Fig. 4e and f. For chromophore 1-*R*, the corresponding global fitting on the 607 and 490 nm traces resulted in one decay component of 229 ps and one rise component of 266 ps. Similarly, a decay lifetime of 141 ps and rise time of 175 ps were estimated for 2-*R*. Accordingly, the efficiency of ISC (Φ_{ISC}) was estimated to be $\Phi_{ISC} = (1/\tau_{rise})/(1/\tau_{decay}) = 0.86$ for 1-*R* and 0.81 for 2-*R*.[33,34] The efficiencies of ISC in 1-*R* and 2-*R* are among the highest values for organic molecules.[35–38] From the energy-optimized structures of 1-*R* and 2-*R* calculated using DFT at the B3LYP/3-21G(d) level, it is

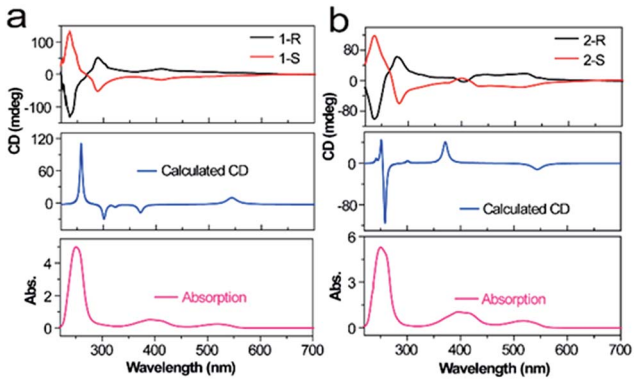

Fig. 2 Comparison of absorption for experimental and theoretically calculated CD spectra of **1** and **2**.

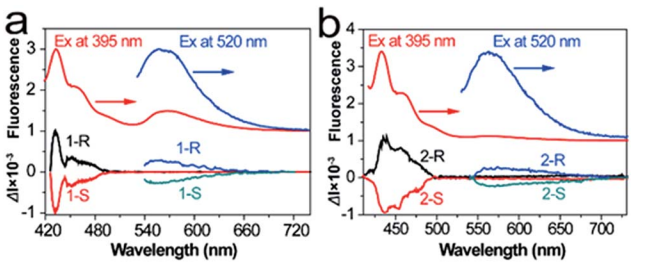

Fig. 3 Comparison of absorption and CPL spectra of (a) **1** and (b) **2** under excitation by different wavelengths.

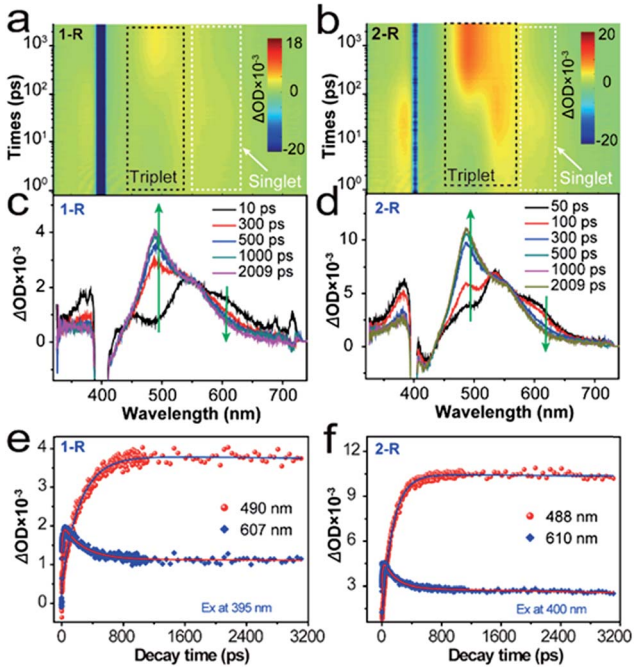

Fig. 4 (a) Full contour plots of fs-TA spectra of 1-*R* (a) and 2-*R* (b) in $CHCl_3$ under excitation by 400 nm light. The most prominent singlet (dash) and triplet (dot-dash) excited state absorption features are outlined for clarity. The black band at ~400 nm originated from the strong pump laser. The Fs-TA spectra of 1-*R* (c) and 2-*R* (d) in $CHCl_3$ at various pump-probe delay times. Kinetic traces and fitting lines of 1-*R* (e) and 2-*R* (f) taken from the singlet and triplet absorption spectra.

apparent that chromophores 1-*R* and 2-*R* exhibit severe out-of-plane distortion that can lead to the breakdown of the σ–π orbital separation, and thus enhance the spin–orbital coupling that is necessary for a highly efficient ISC (inset of Fig. S5†).[39–42] To confirm this, the spin–orbital couplings (ξ_{S1T1}) of **1** and **2** were calculated to be 0.86 cm^{-1} and 0.47 cm^{-1}, respectively (Fig. S7†). These results also account for the low fluorescence quantum yield, proving the generation of the triplet state through a highly efficient ISC pathway.

Low-temperature emission properties of 1-*R* and 2-*R* were studied to obtain their singlet and triplet energy gaps (Δ_{EST}). As shown in Fig. S8,† through the comparison of the fluorescence and phosphorescence bands, equivalent values of Δ_{EST} for 1-*R* and 2-*R* were estimated, *i.e.*, 0.42 eV for both 1-*R* and 2-*R*. Such a low value of Δ_{EST} is quite favourable for the singlet-to-triplet ISC process with high efficiency.[43] Comparisons between 1-*R* and 2-*R* suggest that the substituents can slightly influence their ISC properties. The 1-phenylethylamine group can boost the efficient ISC pathway with the aid of a great ξ_{ST}, where the spin–orbit interaction mixes two states that differ in both spin and electronic configurations. The aforementioned results clearly prove a highly efficient ISC process and the consequential singlet oxygen generation for 1-*R* and 2-*R* upon direct optical excitation. We also measured the actual efficiencies of $^1O_2$ generation (Φ_Δ) for chromophores **1** and **2** in water by using the commercial photosensitizer 5,10,15,20-tetrakis(1-methyl-4-pyridinio)porphyrin tetra(*p*-toluenesulfonate) ($TMPyP_4$) as a standard ($\Phi_r = 0.74$ in water), and the measurement details are described in the ESI.†[19,44] Values of $\Phi_\Delta = 0.73$ and 0.69 were obtained for 1-*R* and 2-*R*, respectively, after 400 nm light irradiation.

It has been reported that most organic molecules exhibit low Φ_Δ in solvents with high polarity and are even insoluble in water.[45–48] The good solubilities of **1** and **2**, as well as their high Φ_Δ values in water, indicate that they are promising candidates for use in PDT. Considering the higher value of Φ_Δ for 1-*R*, we selected it as the photosensitizer to demonstrate the proof-of-concept for PDT application. The specific cellular target of 1-*R* was further confirmed by colocalization assays. The excellent overlap between 1-*R* and commercial lysosome Tracker Red (Lyso) suggests that 1-*R* localises in the lysosome (Fig. 5a). Given the key role of reactive oxygen species (ROS, *e.g.*, $^1O_2$) in PDT, we first verified the ability of 1-*R* to generate intracellular ROS by determining the fluorescence of an ROS tracker, 2,7-dichlorofluorescein diacetate (DCF-DA), which was based on the fact that nonfluorescent DCF-DA can be oxidized by ROS into green-emissive DCF.[49] No obvious fluorescence was observed prior to irradiation (Fig. 5b), whereas significantly enhanced fluorescence occurred along with the increasing irradiation time under a white light emitting diode, demonstrating the intracellular ROS generation by 1-*R*. By employing a calcein AM (living cell) and propidium iodide (PI, dead cell) cellular viability kit, we can distinguish the dead cells from the living cells and visually clarify the PDT effect (Fig. 5c).[50] Upon either light irradiation or 1-*R* exposure alone, most of the cells showed great cellular viability, which demonstrated the resistance of cells to light irradiation and the low dark-cytotoxicity of 1-*R*. With both light irradiation and 1-*R* exposure, the significantly changed morphology of cells and red

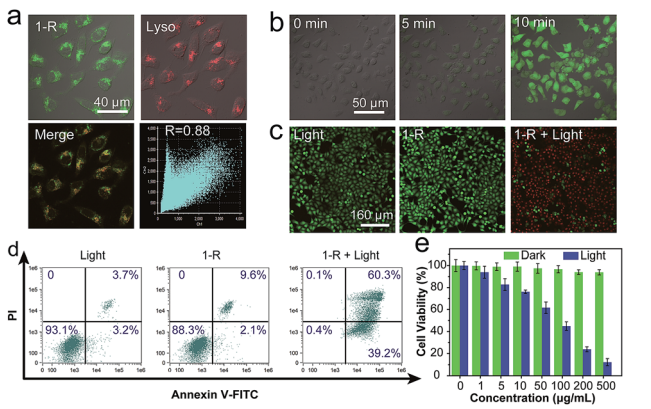

Fig. 5 (a) Colocalization fluorescence images of 1-*R*- and lysosome-tracker (Lyso)-incubated HeLa cells. (b) Images of intracellular ROS generation in 1-*R*-incubated HeLa cells (20 μM) at different irradiation times. (c) Cellular viability assay for HeLa cells incubated with 1-*R* (20 μM). Live cells were labeled with green coloration, whereas dead cells were labeled with red coloration. (d) Flow cytometric assay for studying the PDT effect of 1-*R*. Annexin V-$FITC^-$/PI^- and Annexin V-$FITC^+$/PI^- represent viable and early-stage apoptotic cells, respectively. Annexin V-$FITC^+$/PI^+ indicates later-stage apoptotic or necrotic cells. (e) Cell viability of 1-*R*-incubated HeLa cells with and without light irradiation.

fluorescence confirmed the excellent therapeutic effects of 1-*R*. Then, we conducted a typical flow cytometric assay with HeLa cells to quantitatively evaluate the PDT effect (Fig. 5d). After treatment with either light irradiation or 1-*R* alone, the HeLa cells exhibited cell viability of >88% (Annexin V-FITC$^-$/PI$^-$), again indicating their high resistance to light irradiation and the low dark-cytotoxicity of 1-*R*. However, upon exposure to light irradiation and 1-*R*, the population of early- (39%, Annexin V-FITC$^+$/PI$^-$) and late-stage (60%, Annexin V-FITC$^+$/PI$^+$) apoptotic HeLa cells significantly increased, which was induced by the highly efficient PDT effect of 1-*R*. Moreover, the efficient PDT effect of 1-*R* can be further revealed by the MTT assay (Fig. 5e). It can be concluded that 1-*R* is a promising candidate with potential for application in PDT.

Conclusions

In conclusion, we designed and synthesized chiral and water-soluble tetrazine derivatives **1** and **2**. We observed unusual CPL from the S_2 states, which violates Kasha's rule and results from the large values of the energy gaps between the S_0 and S_2 states. Although the g_{lum} values are in the typical range for simple molecules, the achievement of CPL from upper-excited states is reported for the first time. We also noted that the studied compounds with severely distorted molecular geometries exhibit remarkable ISC and efficient $^1O_2$ generation. Finally, we demonstrated a proof-of-concept application of 1-*R* for PDT. The present work may lead to a new generation of simple molecules with overall performance superior to that of conventional agents in terms of CPL from upper-excited states, $^1O_2$ quantum yield, water dispersibility, and biocompatibility.

Experimental

Steady-state spectroscopy

The UV-visible absorption measurements were carried out using a UV-vis-NIR spectrophotometer (Lambda 950, PerkinElmer, Inc.), while the fluorescence spectra were collected with a spectrometer (Zolix, SENS-9000). CD measurements were conducted on a JASCO J-1500 CD spectrometer, and CPL measurements were performed on a JASCO CPL-300 spectrometer.

Measurements of the fs-TA spectrum

The fs-TA spectra and dynamics were recorded using a standard pump–probe configuration at 350 nm, ~100 fs pump pulses at a 1 kHz repetition rate and a broadband white-light supercontinuum probe (18SI80466 Rev.1, Newport). The excited spot diameter was 300 μm, and the measured quantity was the normalized transmission change, *i.e.*, $\Delta A/A$, which was performed on sample solutions with an optical density below 1 at the excitation wavelength.

Photodynamic therapy activity on cancer cells

The experimental details are described in the ESI.†

Conflicts of interest

The authors declare no conflict of interest.

Acknowledgements

This research was financially supported by the National Natural Science Foundation of China (NSFC Grant no. 11404219, and 61805118) and the Shenzhen Basic Research Project of Science and Technology under Grant No. JCYJ20170302142433007 and the Natural Science Foundation of Guangdong Province (2018A030310637), the Natural Science Foundation of Jiangsu Province of China (No. BK20171020), the China Postdoctoral Science Foundation (No. 2017M621733 and 2018T110488), and the open research fund of the Key Laboratory for Organic Electronics and Information Displays. We gratefully acknowledge the supports from the Instrumental Analysis Center of Shenzhen University (Xili Campus).

Notes and references

1 Y. Shen, Y. Yao, A. N. Brigeman, H. Kim and N. C. Giebink, *Nano Lett.*, 2018, **18**, 1693–1698.
2 W. Cha, W. Kim, H. Mori, T. Yoneda, A. Osuka and D. Kim, *J. Phys. Chem. Lett.*, 2017, **8**, 3795–3799.
3 J. O. Kim, Y. Hong, T. Kim, W. Cha, T. Yoneda, T. Soya, A. Osuka and D. Kim, *J. Phys. Chem. Lett.*, 2018, **9**, 4527–4531.
4 R. García, S. More, M. Melle-Franco and A. Mateo-Alonso, *Org. Lett.*, 2014, **16**, 6096–6099.
5 J. Sung, P. Kim, S. Saga, S. Hayashi, A. Osuka and D. Kim, *Angew. Chem., Int. Ed.*, 2013, **52**, 12632–12635.
6 D. W. Cho, M. Fujitsuka, J. H. Ryu, M. H. Lee, H. K. Kim, T. Majimabc and C. Ima, *Chem. Commun.*, 2012, **48**, 3424–3426.
7 J. Szmytkowski, S. M. K. Brunet, U. Tripathy, J. A. O'Brien, M. F. Paige and R. P. Steer, *Chem. Phys. Lett.*, 2011, **501**, 278–282.
8 M. Beer and H. C. Longuet-Higgins, *J. Chem. Phys.*, 1955, **23**, 1390.
9 M. H. Hui, P. D. Mayo, R. Suau and R. W. Ware, *Chem. Phys. Lett.*, 1975, **31**, 257–263.
10 M. Li, S. H. Li, D. Zhang, M. Cai, L. Duan, M. K. Fung and C.-F. Chen, *Angew. Chem., Int. Ed.*, 2018, **57**, 2889–2893.
11 M. Naito, K. Iwahori, A. Miura, M. Yamane and I. Yamashita, *Angew. Chem., Int. Ed.*, 2010, **49**, 7006–7009.
12 T. Otani, A. Tsuyuki, T. Iwachi, S. Someya, K. Tateno, H. Kawai, T. Saito, K. S. Kanyiva and T. Shibata, *Angew. Chem., Int. Ed.*, 2017, **56**, 3906–3910.
13 J. Cheng, J. Hao, H. Liu, J. Li, J. Li, X. Zhu, X. Liu, K. Wang and T. He, *ACS Nano*, 2018, **12**, 5341–5350.
14 E. M. Sánchez-Carnerero, F. Moreno, B. L. Maroto, A. R. Agarrabeitia, M. J. Ortiz, B. G. Vo, G. Muller and S. Moya, *J. Am. Chem. Soc.*, 2014, **136**, 3346–3349.
15 Y. Inoue, D. Sakamaki, Y. Tsutsui, M. Gon, Y. Chujo and S. Seki, *J. Am. Chem. Soc.*, 2018, **140**, 7152–7158.
16 J. Kumar, T. Nakashima, H. Tsumatori and T. Kawai, *J. Phys. Chem. Lett.*, 2014, **5**, 316–321.

17 C. Ji, Q. Gao, X. Dong, W. Yin, Z. Gu, Z. Gan, Y. Zhao and M. Yin, *Angew. Chem., Int. Ed.*, 2018, **57**, 11384–11388.
18 E. Ju, K. Dong, Z. Chen, Z. Liu, C. Liu, Y. Huang, Z. Wang, F. Pu, J. Ren and X. Qu, *Angew. Chem., Int. Ed.*, 2016, **55**, 11467–11471.
19 W. Hu, M. Xie, H. Zhao, Y. Tang, S. Yao, T. He, C. Ye, Q. Wang, X. Lu, W. Huang and Q. Fan, *Chem. Sci.*, 2018, **9**, 999–1005.
20 H. Uoyama, K. Goushi, K. Shizu, H. Nomura and C. Adachi, *Nature*, 2012, **492**, 234–238.
21 Y. Nakakuki, T. Hirose, H. Sotome, H. Miyasaka and K. Matsuda, *J. Am. Chem. Soc.*, 2018, **140**, 4317–4326.
22 A. Bedi, L. J. W. Shimon and O. Gidron, *J. Am. Chem. Soc.*, 2018, **140**, 8086–8090.
23 C. Zhou, Y. Ren, J. Han, X. Gong, Z. Wei, J. Xie and R. Guo, *J. Am. Chem. Soc.*, 2018, **140**, 9417–9425.
24 N. J. Schuster, R. H. Sánchez, D. Bukharina, N. A. Kotov, N. Berova, F. Ng, M. L. Steigerwald and C. Nuckolls, *J. Am. Chem. Soc.*, 2018, **140**, 6235–6239.
25 C. Allain, J. Piard, A. Brosseau, M. Han, J. Paquier, T. Marchandier, M. Lequeux, C. Boissière and P. Audebert, *ACS Appl. Mater. Interfaces*, 2016, **8**, 19843–19846.
26 Y. H. Gong, F. Miomandre, R. Méallet-Renault, S. Badré, L. Galmiche, J. Tang, P. Audebert and G. Clavier, *Eur. J. Org. Chem.*, 2009, **2009**, 6121–6128.
27 Z. Yang and J. Zhou, *J. Am. Chem. Soc.*, 2012, **134**, 11833–11835.
28 C. Wu, M. S. Coumar, C. Chu, W. Lin, Y. Chen, C. Chen, H. Shiao, S. Rafi, S. Wang, H. Hsu, C. Chen, C. Chang, T. Chang, T. Lien, M. Fang, K. Yeh, C. Chen, T. Yeh, S. Hsieh, J. T.-A. Hsu, C. Liao, Y. Chao and H. Hsieh, *J. Med. Chem.*, 2010, **53**, 7316–7326.
29 Q. Shen, T. Ogata and J. F. Hartwig, *J. Am. Chem. Soc.*, 2008, **130**, 6586–6596.
30 Q. Shen, S. Shekhar, J. P. Stambuli and J. F. Hartwig, *Angew. Chem., Int. Ed.*, 2005, **44**, 1371–1375.
31 J. E. Field, G. Muller, J. P. Riehl and D. Venkataraman, *J. Am. Chem. Soc.*, 2003, **125**, 11808–11809.
32 A. Satrijo, S. C. J. Meskers and T. M. Swager, *J. Am. Chem. Soc.*, 2006, **128**, 9030–9031.
33 K. Nagarajan, A. R. Mallia, K. Muraleedharan and M. Hariharan, *Chem. Sci.*, 2017, **8**, 1776–1782.
34 Y. Wu, Y. Zhen, Y. Ma, R. Zheng, Z. Wang and H. Fu, *J. Phys. Chem. Lett.*, 2010, **1**, 2499–2502.
35 F. Hu, S. Xu and B. Liu, *Adv. Mater.*, 2018, **30**, 1801350.
36 W. Piao, K. Hanaoka, T. Fujisawa, S. Takeuchi, T. Komatsu, T. Ueno, T. Terai, T. Tahara, T. Nagano and Y. Urano, *J. Am. Chem. Soc.*, 2017, **139**, 13713–13719.
37 Z. Wang, J. Zhao, A. Barbon, A. Toffoletti, Y. Liu, Y. An, L. Xu, A. Karatay, H. G. Yaglioglu, E. A. Yildiz and M. Hayvali, *J. Am. Chem. Soc.*, 2017, **139**, 7831–7842.
38 R. Acharya, S. Cekli, C. J. Zeman, R. M. Altamimi and K. S. Schanze, *J. Phys. Chem. Lett.*, 2016, **7**, 693–697.
39 W. Zhao, Z. He, Q. Peng, J. W. Y. Lam, H. Ma, Z. Qiu, Y. Chen, Z. Zhao, Z. Shuai, Y. Dong and B. Z. Tang, *Nat. Commun.*, 2018, **9**, 3044.
40 Y. Cakmak, S. Kolemen, S. Duman, Y. Dede, Y. Dolen, B. Kilic, Z. Kostereli, L. T. Yildirim, A. L. Dogan, D. Guc and E. U. Akkaya, *Angew. Chem., Int. Ed.*, 2011, **50**, 11937–11941.
41 K. Nagarajan, A. R. Mallia, V. S. Reddy and M. Hariharan, *J. Phys. Chem. C*, 2016, **120**, 8443–8450.
42 K. Nagarajan, A. R. Mallia, K. Muraleedharan and M. Hariharan, *Chem. Sci.*, 2017, **8**, 1776–1782.
43 S. Cekli, R. W. Winkel, E. Alarousu, O. F. Mohammed and K. S. Schanze, *Chem. Sci.*, 2016, **7**, 3621–3631.
44 Z. An, C. Zheng, Y. Tao, R. Chen, H. Shi, T. Chen, Z. Wang, H. Li, R. Deng, X. Liu and W. Huang, *Nat. Mater.*, 2015, **14**, 685.
45 R. Gao, X. Mei, D. Yan, R. Liang and M. Wei, *Nat. Commun.*, 2018, **9**, 2798.
46 N. N. Esemoto, Z. Yu, L. Wiratan, A. Satraitis and M. Ptaszek, *Org. Lett.*, 2016, **18**, 4590–4593.
47 L. Shi, B. Hernandez and M. Selke, *J. Am. Chem. Soc.*, 2006, **128**, 6278–6279.
48 L. Beverina, M. Crippa, M. Landenna, R. Ruffo, P. Salice, F. Silvestri, S. Versari, A. Villa, L. Ciaffoni, E. Collini, C. Ferrante, S. Bradamante, C. M. Mari, R. Bozio and G. A. Pagani, *J. Am. Chem. Soc.*, 2008, **130**, 1894–1902.
49 L. Huang, Z. Li, Y. Zhao, Y. Zhang, S. Wu, J. Zhao and G. Han, *J. Am. Chem. Soc.*, 2016, **138**, 14586–14591.
50 H. Zhao, W. Hu, H. Ma, R. Jiang, Y. Tang, Y. Ji, X. Lu, B. Hou, W. Deng and W. Huang, *Adv. Funct. Mater.*, 2017, **27**, 1702592.